THE JOURNAL OF PHYSICAL CHEMISTRY A

ARTICLE

pubs.acs.org/JPCA

Ultrafast Branching of Reaction Pathways in 2-(2′-Hydroxyphenyl)benzothiazole in Polar Acetonitrile Solution

Omar F. Mohammed,[†] Sandra Luber,[‡] Victor S. Batista,[‡] and Erik T. J. Nibbering*[,†]

[†]Max Born Institut für Nichtlineare Optik und Kurzzeitspektroskopie, Max Born Strasse 2A, D-12489 Berlin, Germany

[‡]Department of Chemistry, Yale University, P.O. Box 208107, New Haven, Connecticut 06520-8107, United States

ABSTRACT: In a combined study on the photophysics of 2-(2′-hydroxyphenyl)-benzothiazole (HBT) in polar acetonitrile utilizing ultrafast infrared spectroscopy and quantum chemical calculations, we show that a branching of reaction pathways occurs on femtosecond time scales. Apart from the excited-state intramolecular hydrogen transfer (ESIHT) converting electronically excited enol tautomer into the keto tautomer, known to be the dominating mechanism of HBT in nonpolar solvents such as cyclohexane and tetrachloroethene, in acetonitrile solution twisting also occurs around the central C−C bond connecting the hydroxyphenyl and benzothiazole units in both electronically excited enol and keto tautomers. The solvent-induced intramolecular twisting enables efficient internal conversion pathways to both enol and keto tautomers in the electronic ground state. Whereas relaxation to the most stable enol tautomer with twisting angle Θ = 0° implies full ground state recovery, a small fraction of HBT molecules persists as the keto twisting conformer with the twisting angle Θ = 180° for delay times extending beyond 120 ps.

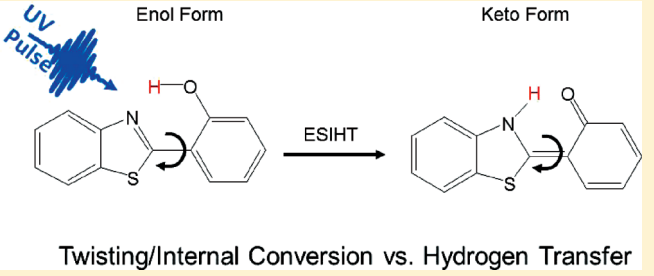

1. INTRODUCTION

Branching of chemical reactions means a multiple outcome in reaction products. For molecular reactants converting into products in their respective electronic ground states, branching may be caused by the existence of several energetically accessible states.[1,2] Photoinduced reactions exhibiting branching into several products are less numerous. Even though the observation of state-selective quantum yield for reaction products has been reported,[3] the number of studies on the time-resolved observation of the formation dynamics of different (transient) molecular product species have remained scarce. Here one can distinguish between cases where the different bond-breaking reaction channels are chemically identical (see, e.g., refs 3−6) and a fully asymmetric outcome of the reactions, with chemically distinct products.[7,8] Optimal control of the outcome of chemical reaction dynamics has been pursued using amplitude and phase modulated excitation pulses on molecular systems. For midsized organic molecules, control has been hampered due to the onset of intramolecular vibrational redistribution (IVR).[9,10] Control of reaction dynamics in the condensed phase is even more difficult to achieve, as the solute−solvent interactions often have much more impact on the molecular dynamical evolution than what can be achieved with preparation of excited states using laser pulses. In fact, solute−solvent interactions have a profound influence on quantum yields of photoinduced trans/cis isomerizations,[11,12] much more than has been achieved with laser control experiments.[13−15]

Until now, femtosecond studies of ultrafast branching pathway dynamics have mostly dealt with chemical bond disruption/formation, and less with other elementary chemical transformations such as electron, proton, or hydrogen transfer and trans/cis isomerizations.[16] In this work we report on the ultrafast photoinduced dynamics of 2-(2′-hydroxyphenyl)-benzothiazole (HBT) in acetonitrile (ACN). HBT is one of the benchmark systems for excited-state intramolecular hydrogen transfer (ESIHT).[17−27] Here the chemical reaction coordinate is that of enol → keto conversion by intramolecular hydrogen transfer (see Scheme 1) via an intramolecular hydrogen bond connecting the hydroxyphenyl and benzothiazole moieties. In nonpolar solvents, HBT solely exists in its enol form (twisting angle around the central bond connecting the hydroxyphenyl and benzothiazole moieties Θ = 0°) with this intramolecular hydrogen bond present. Photoinduced chemistry of HBT then exclusively implies electronic excitation of the enol(Θ = 0°) state, followed by an ultrafast hydrogen transfer from enol*(Θ = 0°) to keto*(Θ = 0°) on a time scale of 60 fs.[19,21−27] A fluorescence signal with a high quantum yield (300 ps time constant[19]) indicates the conversion of HBT into the keto(Θ = 0°) electronic ground state, followed by intramolecular hydrogen back-transfer to the enol(Θ = 0°) ground state, completing the photocycle.

We now present experimental and theoretical results of analyzing the ultrafast dynamics of HBT in ACN, and conclude that even though in polar ACN HBT in the electronic ground state only exists in the enol(Θ = 0°) geometry, electronic

Received: March 10, 2011
Revised: May 22, 2011
Published: May 23, 2011

Scheme 1. The Molecular Structures [DFT(BP86/RI)/TZVPP/COSMO] of the Enol Isomer (Left-Hand Side) in the Θ = 0° Conformation and the Keto Isomer (Right-Hand Side) in the Θ = 180° Conformation of HBT[a]

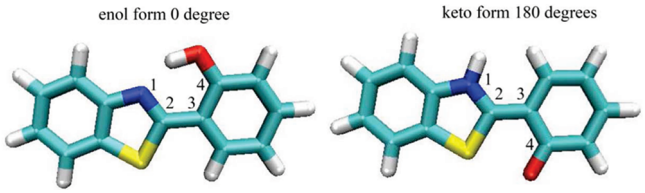

[a] The twisting degree of freedom around the central C2−C3 bond connecting the hydroxyphenyl and benzothiazole moieties of HBT is defined in this work as the twisting angle Θ between the atoms N1−C2−C3−C4.

excitation to the enol*(Θ = 0°) state is followed by a branching into two different reaction coordinates: the aforementioned ESIHT coordinate resulting in the keto*(Θ = 0°) conformation, and the twisting coordinate around the central C−C bond connecting the hydroxyphenyl and benzothiazole units, facilitating internal conversion back to the enol(Θ = 0°) ground state. The twisting state is concluded to shorten the lifetime of the keto*(Θ = 0°) state as well, as derived from the kinetics of IR-active fingerprint modes for the keto*(Θ = 0°) and keto(Θ = 180°) states.

2. EXPERIMENTAL AND THEORETICAL DETAILS

2.1. Steady-State and Time-Resolved Experiments. Steady-state electronic absorption spectra were recorded with a double-beam UV−vis spectrometer (Perkin-Elmer), and emission spectra were recorded with a spectrofluorometer (Spex Fluorolog). Perdeuterated acetonitrile (ACN-d_3) was obtained from Deutero GmbH (99.96% deuteration grade, water content <0.03%), while the solvents ACN, tetrachloroethylene (TCE, water content <0.01%), and HBT were purchased from Sigma-Aldrich. For the steady-state spectra, HBT was sublimed and subsequently dried over P_2O_5 under vacuum conditions. With this procedure, no significant amounts of water were present in the HBT samples, as evidenced by the recorded steady-state IR spectra. No differences were observed in the HBT spectra when using ACN or ACN-d_3. All experiments were performed at room temperature (24 ± 2 °C).

Ultrafast mid-Infrared (IR) spectroscopy was performed using a home-built 1 kHz Ti:sapphire regenerative and multipass amplifier, followed by parametric conversion of the laser output into UV pump pulses, centered at 330 nm with pulse energies above 2 μJ and pulse durations of 50 fs, and tunable mid-IR probe pulses of 100−150 fs duration. For details on the experimental setup, we refer to a previously published report.[26]

The molecular structures were optimized with the quantum chemical package Turbomole,[28] version 6.2. For all calculations presented in this work (except where electronic transition dipoles were estimated), density functional theory (DFT) was employed with the BP86 density functional[29,30] and Ahlrichs' TZVPP basis set.[31,32] The normal modes, frequencies, and IR intensities as well as the change of the electric dipole moments with respect to selected normal coordinates presented in Figure 7 were obtained with SNF[33,34] in the harmonic approximation. SNF acts as a meta-program that collects raw data provided by Turbomole and provides a restart-friendly and massively parallelized implementation. Electronic energy gradients and electric dipole moments were calculated with Turbomole for distorted structures of the molecule under consideration, and the normal modes and IR intensities were obtained by SNF using numerical differentiation. A three-point central difference formula[35] was used and the step length for the differentiation was set to 0.01 Bohr. As shown in, e.g., refs 36−38, harmonic BP86 vibrational frequencies match experimental fundamental ones well. The resolution of the identity (RI) density-fitting technique was employed for all calculations with the BP86 density functional with Turbomole using the Karlsruhe auxiliary basis functions.[39] As a continuum model, we employed COSMO[40] with the standard settings as implemented in Turbomole except for the permittivity, which was set to 37.5 (compare ref 41). The spectra were broadened with a Gaussian band shape and a full width at half-maximum height of 15 cm^{-1}. The frequencies used in the calculated spectra presented in Figure 9 were scaled by a factor of 1.01, and the intensities of the line spectra in Figure 8 were scaled by a factor of 0.08. Molecular structures, normal modes, and (transition) dipoles were visualized using the programs VMD[42] and Gaussview.[43]

3. RESULTS AND DISCUSSION

3.1. Steady-State Experiments. In Figure 1a we show the steady-state UV/vis spectra of HBT in TCE and in ACN. As reported before,[18,25,26] the electronic absorption band of HBT in TCE is located between 310 and 360 nm, whereas the electronic emission band is strongly red-shifted, peaking at 540 nm. These features have been understood to be indicative of the photocycle where HBT is electronically excited in its enol form (with intramolecular hydrogen bond, i.e., Θ = 0°), i.e., S_0 enol(Θ = 0°) → S_1 enol*(Θ = 0°), followed by ultrafast ESIHT leading to the S_1 keto*(Θ = 0°) state. The S_1 keto*(Θ = 0°) state has a lifetime of 300 ps in TCE.[18] On this time scale, HBT emits a fluorescent photon, converting S_1 keto*(Θ = 0°) into S_0 keto (Θ = 0°), which subsequently changes by back intramolecular hydrogen transfer into the enol (Θ = 0°) form, closing the photocycle.

In ACN, HBT has a similar electronic absorption spectrum, indicative of the S_0 enol → S_1 enol* transition, about 10 nm blue-shifted. The reason for this solvation by the polar ACN solvent, or by the intramolecular hydrogen bond broken by the solvent, and the possible existence of different geometries of HBT in the enol form, with the twisting angle Θ as an additional degree of freedom, will be answered here. The emission spectrum of HBT upon electronic excitation at 330 nm, however, is drastically different from that of HBT in TCE. Besides an emission band at 540 nm, indicative of S_1 keto* → S_0 keto fluorescence, a band of similar emission strength is found peaking at 375 nm, strongly suggesting that S_1 enol* → S_0 enol fluorescence also occurs in HBT in ACN solution. The overall emission strength of HBT in ACN is a factor of ∼30 times less than that observed in TCE under identical excitation conditions, hinting at a pronounced electronic excited state lifetime shortening of HBT (regardless of the actual tautomer present) when comparing ACN and TCE solvents. This is in accordance with reported lifetimes of HBT in ACN (14 ps) and in TCE (300 ps).[19] As such, the choice of polar ACN as the solvent opens one or even several nonradiative decay channels for electronically excited HBT.

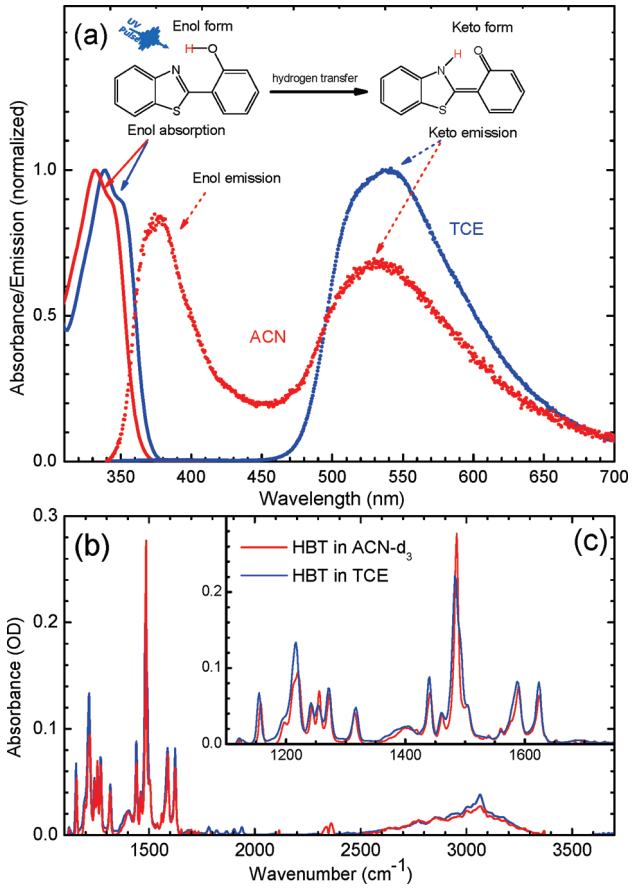

Figure 1. (a) Reaction scheme of photoinduced enol-keto tautomerism of HBT and the UV/vis absorption and emission spectra of HBT in TCE and ACN. (b) Steady-state IR spectra of HBT in TCE and ACN-d_3. (c) The inset highlights the fingerprint region investigated in the time-resolved experiment.

Steady-state IR spectroscopy of HBT in TCE[25,26] and in ACN-d_3 solution are compared in Figure 1b. Here it is shown that the IR-active vibrations of HBT in TCE and in ACN-d_3 are fully identical, both for the vibrational fingerprint modes between 1000 and 1800 cm^{-1} and for the OH stretching band, extending between 2500 and 3300 cm^{-1}. In particular, the fact that the OH stretching band, as well as those fingerprint modes where the O−H bending motion is contributing, do not change when HBT is dissolved in polar ACN instead of in nonpolar TCE clearly shows that electronic ground-state HBT is predominantly present in the enol($\Theta = 0°$) geometry in ACN. As we will discuss in Section 3.3, enol geometries with the intramolecular hydrogen bond broken and with different twisting angles, as well as with the OH-group hydrogen bonded to a solvent molecule, would exhibit different vibrational patterns. This finding is important, as it significantly limits the number of possible photocycle scenarios of HBT in ACN.

3.2. Ultrafast UV-pump IR-Probe Spectroscopy of HBT in ACN-d_3. In Figure 2 we compare the transient IR pump−probe spectra of HBT in TCE and in ACN-d_3. With such a comparison it becomes immediately clear that the ultrafast photoinduced dynamics of HBT is strongly different in the two solvents. Upon UV excitation of HBT in TCE (Figure 2a) within time resolution (~150 fs), the vibrational marker bands of the S_1 keto*($\Theta = 0°$) state are prominent throughout the fingerprint range from 1250

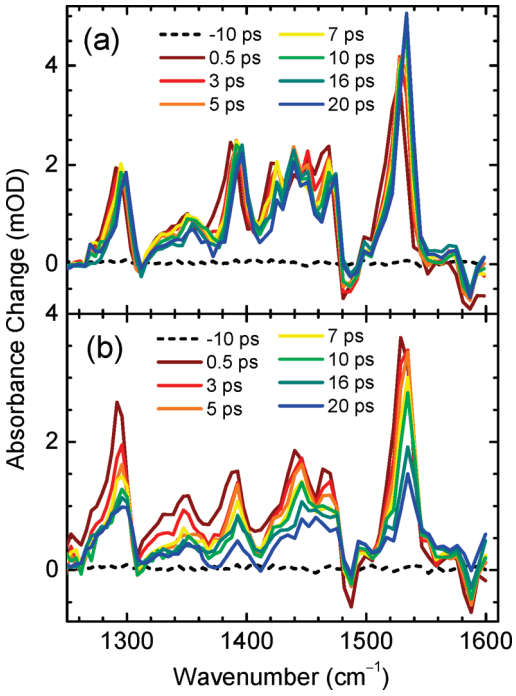

Figure 2. Transient IR spectra of HBT in the fingerprint region measured in (a) TCE and in (b) ACN-d_3 solution after excitation at 330 nm with a 50 fs pump pulse.

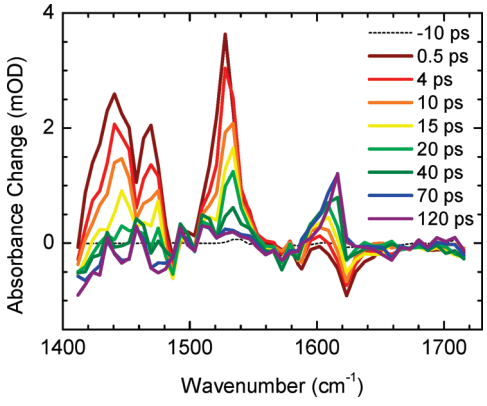

Figure 3. Transient IR spectra of HBT in ACN-d_3, showing the S_0 enol bleach and S_1 keto* marker bands at early pulse delays, and the subsequent excited state decay, enol bleach fill, and the transient appearance of a marker band at 1616 cm^{-1} of a nonequilibrium HBT conformer.

to 1600 cm^{-1}, and only exhibit a frequency upshifting on a time scale of several tens of picoseconds, indicative of vibrational cooling of the S_1 keto*($\Theta = 0°$) state.[25,26] For HBT in ACN-d_3 (Figure 2b), the same marker bands appear within time resolution, followed again by a frequency upshifting on picosecond time scales likely caused by vibrational cooling. This suggests that photoinduced enol*→keto* tautomerism of HBT is as fast in ACN-d_3 as it is in TCE. However, a pronounced decay of these fingerprint bands of excited state HBT takes place on the same time scale as that of vibrational cooling effects. This decay indicates that the lifetime of the S_1 keto* state is severely shortened in ACN-d_3 as compared to that in TCE.

dx.doi.org/10.1021/jp202277t |J. Phys. Chem. A 2011, 115, 7550–7558

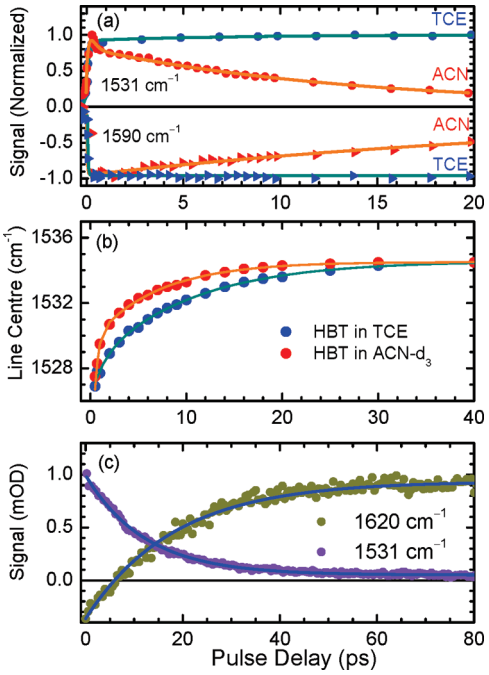

Figure 4. Kinetics of some of the vibrational marker modes of HBT in TCE and in ACN-d_3 (experimental data are given by the symbols, biexponential fits are depicted as solid lines). (a): Transient absorption at 1531 cm^{-1} showing the dynamics in the S_1 keto* state and transient bleach at 1586 cm^{-1}, indicative of the recovery of the S_0 enol state in ACN-d_3; (b) time-dependence of the frequency position of the strongest marker mode of the S_1 keto* state; (c) the decay of the transient absorption at 1531 cm^{-1} and the rise of absorption of 1620 cm^{-1}, suggesting that the decay of the S_1 keto* state correlates with the appearance of a transient species with lifetime extending beyond 100 ps.

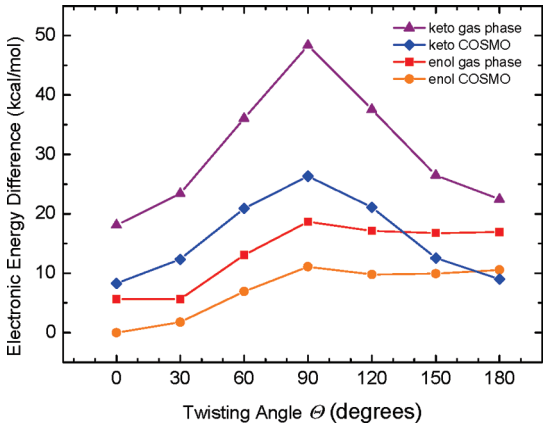

Figure 5. Electronic energy difference [DFT(BP86/RI)/TZVPP] of the enol and keto tautomers of HBT in the S_0 state as function of twisting angle Θ, calculated for the conformers in the gas phase, and with inclusion of the solvent continuum model COSMO.

Figure 3 shows the transient absorption of HBT in ACN-d_3 for different pulse delay times in an expanded view. Here at early pulse delay times, besides the strong marker bands of the S_1 keto* state between 1400 and 1550 cm^{-1}, two bleach signals of the S_0 enol(Θ = 0°) state at 1590 and at 1625 cm^{-1} are observable. Interestingly, the temporal behavior of transient absorption in the spectral region of these bleached bands of the S_0 enol(Θ = 0°) state reveals that the S_0 enol(Θ = 0°) state recovers on a time scale of several tens of picoseconds (Figure 4a). However, the appearance of a transient band in the same spectral region, with a rise in magnitude on the same time scale as that it appears to change its transition frequency to higher values, suggests that one or several HBT tautomer species are transiently formed that are structurally different from the S_0 enol(Θ = 0°) state. The appearance of this marker band is initially at 1602 ± 6 cm^{-1} (at 0.4 ps delay), and upshifts to 1616 ± 6 cm^{-1} at 120 ps. Red-shifted vibrational frequencies can often be explained by having the fingerprint marker mode in its v = 0 state, while low-frequency modes anharmonically coupled to this fingerprint mode are substantially populated.[12,44] The formation of this structurally different species is thus accompanied by initial elevated vibrational excitation of its low-frequency modes, suggesting an internal conversion mechanism from the electronic excited state of HBT into, e.g., the ground state or into a triplet state, where a substantial amount of electronic energy is converted into vibrational energy.

Biexponential fitting shows that frequency upshifting of the strongest marker band of the S_1 keto* state, located at 1526 cm^{-1} at 0.5 ps pulse delay and reaching 1535 cm^{-1} at long pulse delays, is faster in ACN-d_3 than in TCE (Figure 4b). Whereas the fast component has a similar time constant of 0.8 ± 0.2 ps, the long time constant is 14.7 ± 2.3 ps in TCE (in accordance with previously reported data[25,26]), whereas it is only 10 ± 3 ps in ACN-d_3. The similarity of the early time components in the two solvents reflects IVR effects. The long time component on the other hand shows that vibrational energy dissipation is faster in ACN-d_3 than in TCE.

The decay of the transient absorption signal marking the S_1 keto* state of HBT in ACN-d_3 at 1531 cm^{-1} (decaying with an exponential time constant of 12.4 ± 0.5 ps) and the rise of the 1616 cm^{-1} marker band of the transient HBT species (fitted with an exponential rise time of 17.8 ± 1.2 ps) appear to be similar to the reported 14 ps excited state lifetime of HBT in ACN (Figure 4c).[19] From this we conclude that the HBT kinetics observed in ACN-d_3 is governed by electronic excited state decay. The fact that not only is a bleach refill of bands of the S_0 enol(Θ = 0°) state observed, but also the appearance of one or more structurally distinct HBT species, suggests that the electronic excited state decay of HBT follows a multitude of different nonradiative relaxation pathways out of the S_1 state.

3.3. Twist Angle Dependence of Enol and Keto Isomers of HBT in the S_0 State. In this section, we determine the stability of different enol and keto isomers of HBT in the S_0 state and the dependence of the IR spectra on the twisting angle Θ, as defined in Scheme 1. To achieve this, we have performed DFT calculations. To investigate whether enol conformers with Θ values other than 0° may be important for the description of the ground state IR spectra of HBT, we performed molecular structure optimizations by taking the enol(Θ = 0°) optimized structure and fixing the twisting angle to Θ = 30°, 60°, 90°, 120°, 150°, and 180°. The corresponding electronic energies are given in Figure 5.

As can be seen in Figure 5, the enol(Θ = 0°) and enol(Θ = 30°) conformers have similar electronic energies in the gas phase. The electronic energy of enol(Θ = 180°) is 11.29 kcal/mol higher than that of the enol(Θ = 0°) conformer, while the enol(Θ = 90°) conformer has the highest electronic energy difference of the enol conformers (13 kcal/mol in the gas phase). A similar electronic energy barrier was calculated taking into

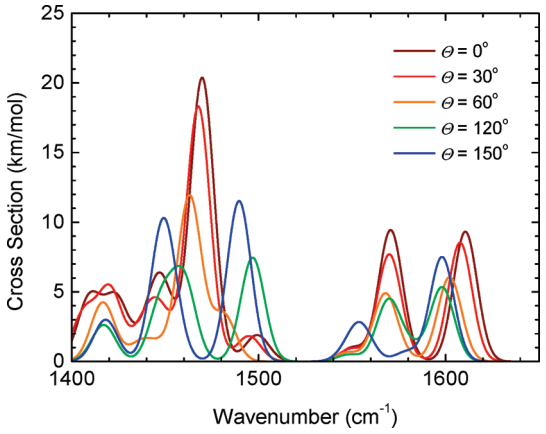

Figure 6. Calculated IR spectra [DFT(BP86/RI)/TZVPP/COSMO] of enol conformers of HBT with different twisting angles Θ.

account solvent effects by inclusion of the continuum model COSMO, where the enol(Θ = 0°) and enol(Θ = 30°) conformers are again the ones with the lowest electronic energy.

In an analogous way, the electronic energies of the keto conformers with Θ values of 0°, 30°, 60°, 90°, 120°, and 150° were obtained by taking the keto(Θ = 180°) optimized structure and fixing the twisting angle to the above-mentioned values. Proceeding in this way, we were able to optimize the keto(Θ = 120°) and (Θ = 150°) conformers in the gas phase. For the other keto conformers in the gas phase, we fixed the hydrogen atom bound to the nitrogen atom in addition to the twisting angle, because otherwise enol forms were obtained after structure optimization. This is, of course, an additional restriction in the calculations. The lowest electronic energies were calculated for the keto(Θ = 180°) and keto(Θ = 0°) conformers, whereas the highest electronic energy was again obtained for the keto(Θ = 90°) conformer.

A similar tendency to form the enol tautomer from the keto tautomer was observed in the optimizations using the continuum model COSMO, where we could only obtain keto conformers for Θ < 90° by fixing the hydrogen atom bound to the nitrogen atom. The energy barrier was found to be around 12 kcal/mol lower than for the keto conformers in the gas phase. We should note that the electronic energies shown in Figure 5 are calculated for a temperature of 0 K, do not consider any vibrational and temperature corrections, and contain no explicit solvent molecules. In addition, it is known that with DFT, difficulties may arise in the proper calculation of rotation around double bonds. However, a good agreement between energies calculated with DFT and with multireference methods was found in ref 45 for the keto form of HBT with twisting angles ranging from Θ = 0° to Θ = 70°. This indicates that our resulting electronic energy values can be used as a qualitative estimate.

Our calculated IR spectra, obtained for the various enol conformers (except for enol(Θ = 90°) and enol(Θ = 180°) for which normal modes with negative frequencies were found) are given in Figure 6. The twisting angle dependence of the vibrational modes of HBT is clearly illustrated with the IR-active transitions in the fingerprint region from 1440 to 1520 cm^{-1}. The enol(Θ = 0°) and enol(Θ = 30°) conformers give rise to an intense band around 1465 cm^{-1} while this band is diminished in case of conformers with other Θ values. Typical for the enol(Θ = 120°) and enol(Θ = 150°) conformers in this part of the IR

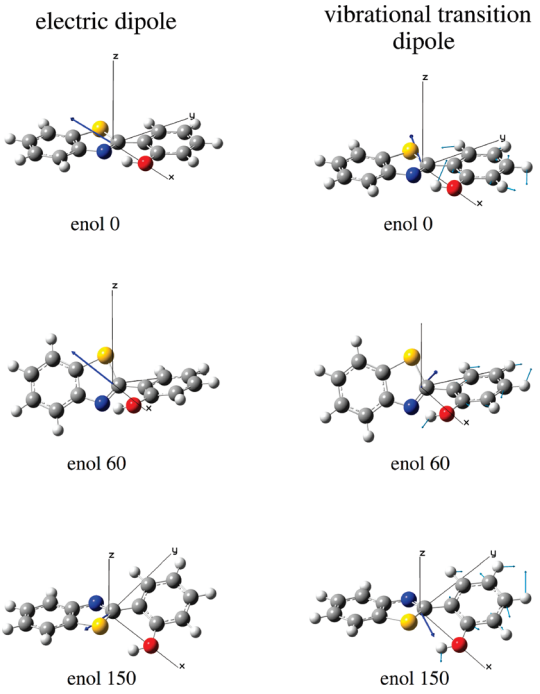

Figure 7. Left-hand side: Electric dipoles (shown as dark blue arrows) of the enol(Θ = 0°), enol(Θ = 60°), and enol(Θ = 150°) conformers of HBT. Right-hand side: Vibrational transition dipoles (dark blue arrows) corresponding to the normal modes (represented by the light blue arrows) at 1571 cm^{-1} for enol(Θ = 0°), at 1568 cm^{-1} for enol(Θ = 60°), and at 1555 cm^{-1} for enol(Θ = 150°).

spectrum is a doublet, whereas the other conformers have three bands, consisting of a relatively intense one surrounded by two weaker ones. All conformers show two bands between 1550 and 1650 cm^{-1}, whereby the one at higher wavenumber is shifted to lower wavenumbers with increasing Θ values. We have plotted the vibrational displacements of the normal mode responsible for the intense band around 1560 cm^{-1} in Figure 7, for the enol(Θ = 0°), enol(Θ = 60°), and enol(Θ = 150°) conformers. This normal mode carries hydrogen bending of the OH group as well as carbon ring stretching and hydrogen bending vibrations of the phenyl-moiety. The change of the electric dipole due to this normal mode, calculated as the derivative of the molecular electric dipole with respect to the corresponding normal coordinate, is also given in Figure 7 and denoted as "vibrational transition dipole". As can be seen by comparison with the electric dipole of the molecule shown on the left-hand side of Figure 7, the electric dipole is significantly altered by this normal mode, i.e., the mode has a large IR cross section.

We report bond lengths for our optimized molecular structure of the enol(Θ = 0°) form in Table 1 (atom numbering according to Scheme 1). These values are comparable to the ones reported in ref 46 where distances were obtained from DFT calculations using the B3LYP density functional[47,48] and the TZVP basis set[32] and from the RI-CC2[49] optimized structure (also using the TZVP basis set;[46] for molecular structures calculated with the Hartree−Fock method, see, e.g., refs 23 and 50). Performing structure optimizations starting from the Θ = 0° and Θ = 180° conformers of the enol and keto tautomers of HBT without fixing any atom or angle, we obtained, besides the enol(Θ = 0°) and keto(Θ = 180°) conformers, a stable enol conformer with a twisting angle of Θ = 153° (gas phase) and Θ = 152° (COSMO).

These results are in contrast to the ones in ref 46, where no energy minimum was found for the keto form in the ground state.

3.4. Solvent Dependence of Fingerprint Modes As Indicated in the Calculated IR Spectra. Since the experimental measurements were performed in the polar ACN solvent, it is important to incorporate solvent effects into the calculations. As a first step, we used the solvent continuum model COSMO. The corresponding spectra of the enol(Θ = 180°) and keto(Θ = 180°) conformers are shown as an example in the lower part of Figure 8.

As illustrated in Figure 8 for the enol tautomer dissolved in a polar medium, application of the continuum model COSMO leads to vibrational frequencies that are shifted to lower values compared to the ones obtained for the enol tautomer in the gas phase. Furthermore, the IR intensities are higher than the ones obtained without the continuum model. However, the overall appearance of the spectra obtained with and without COSMO is quite similar. If an explicit ACN solvent molecule hydrogen-bonded to HBT is, in addition to COSMO, considered in the calculation the IR spectrum changes remarkably (for the molecular structure and corresponding IR-active bands, see Figure 8). The normal mode with an IR-active transition at 1600 cm^{-1} is again shifted to lower frequencies, whereas the one around 1580 cm^{-1} occurs at a similar frequency compared to the calculation with COSMO but excluding an explicit solvent molecule. This can easily be understood since the first normal mode is centered on the hydroxyphenyl moiety and involves stretching displacements of the carbon atoms and a strong bending vibration of the hydrogen atom of the hydroxyl group. The second normal mode is mainly localized on the benzothiazole ring and is thus not much affected by having an explicit ACN molecule hydrogen-bonded to the enol OH group. In an analogous way, the normal mode around 1565 cm^{-1} involves mainly displacements of the hydroxyl group and of ring stretching carbon atoms, so that a shift to higher frequency values is observed when an explicit ACN molecule is included, compared to the calculation solely involving COSMO. The normal mode around 1550 cm^{-1} involves again displacements on the benzothiazole moiety of the molecule, and it is no surprise then that the corresponding vibrational frequencies are not significantly changed by having an ACN molecule hydrogen-bonded to HBT. The region between 1440 and 1500 cm^{-1} shows two bands both with and without consideration of solvent effects, but the order of these normal modes on vibrational frequency gets partially reversed.

As already mentioned, the twisting angle, with its initial value of Θ = 180° in the optimization procedures, was found to relax to Θ = 153° and 152° for the enol conformer optimized in the gas phase and with inclusion of COSMO, respectively. In contrast to that, a value of Θ = 178° was obtained for the HBT—solvent complex. Such a change in twisting angle already drastically

Table 1. Bond Lengths Obtained for HBT Enol(Θ = 0°) in the S_0 State

bond (Å)[a]	DFT, BP86, TZVPP basis set[b]	DFT, B3LYP, TZVP basis set[c]	RI-CC2, TZVP basis set[c]
hydroxyl H—O	1.009	0.990	0.995
N1—hydroxyl H	1.687	1.753	1.716
O—C4	1.344	1.343	1.350
C4—C3	1.429	1.420	1.420
C3—C2	1.449	1.453	1.450
C2—N	1.318	1.304	1.322

[a] Atom numbering according to Scheme 1. [b] This work. [c] Reference 46.

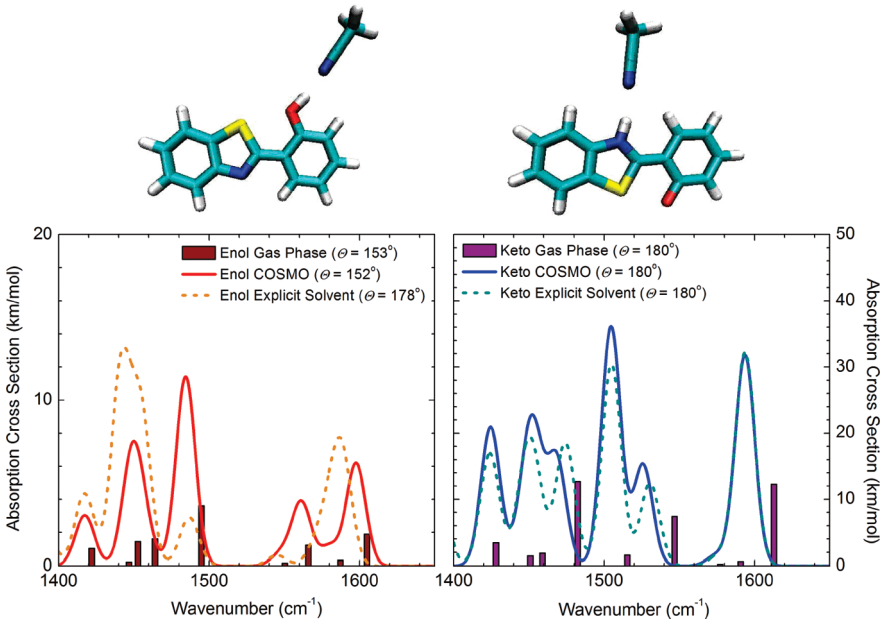

Figure 8. Optimized structures [DFT(BP86/RI)/TZVPP/COSMO] of the enol(Θ = 180°) (left-hand side of upper part) and keto(Θ = 180°) (right-hand side of upper part) conformers of HBT with one ACN molecule hydrogen-bonded to the hydroxyl and amine hydrogen atoms, respectively. Calculated IR spectra [DFT(BP86/RI)/TZVPP] of the optimized enol(Θ) (left-hand side of lower part) and keto(Θ) (right-hand side of lower part) conformers of HBT obtained without inclusion of any solvent effects ("Gas Phase"), with inclusion of the continuum model COSMO ("COSMO"), and by using COSMO and one explicit hydrogen-bonded ACN solvent molecule ("Explicit Solvent"). For enol(Θ), the twisting angles were Θ = 153° for gas phase, Θ = 152° for COSMO, and Θ = 178° for COSMO with an explicit ACN molecule hydrogen-bonded to HBT. For keto(Θ), the twisting angle was ketoΘ = 180° for all cases.

dx.doi.org/10.1021/jp202277t |J. Phys. Chem. A 2011, 115, 7550–7558

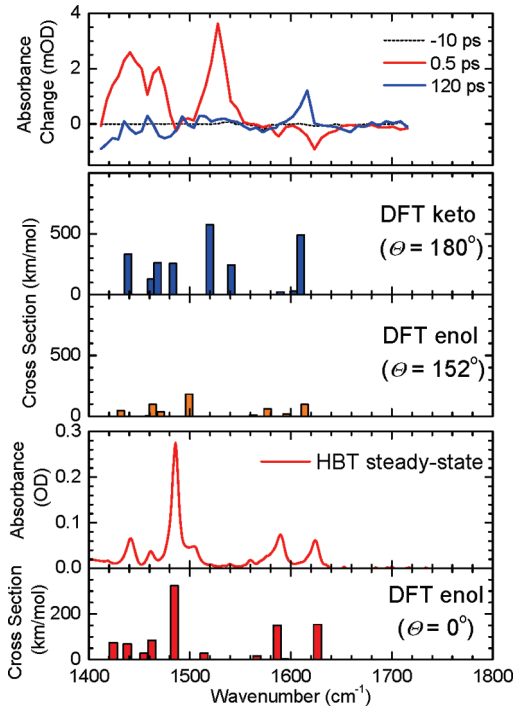

Figure 9. Comparison of the transient IR spectra at early and long delays around 1500−1650 cm^{-1} with calculated spectra (DFT(BP86/RI)/TZVPP/COSMO) of the enol and keto species with varying twisting angle Θ, as well as a comparison of the steady-state IR spectrum of HBT in ACN-d_3, which can be fully explained with the vibrational mode pattern of S_0 enol(Θ = 0°) calculated with DFT.

affects the calculated IR spectrum; in addition, the effects of the existing solute−solvent hydrogen bond play a role.

The situation is different in the case of the keto(Θ = 180°) conformer. Independent of the inclusion of solvent effects, a twisting angle of Θ = 180° was obtained for the three optimized molecular structures employed for the spectra calculations, as shown in Figure 8. Contrary to the spectra of the enol(Θ = 180°) conformer, the largest differences were found between the gas phase and the COSMO calculations. Inclusion of an explicit ACN molecule, which is hydrogen bonded to the amine hydrogen atom (see Figure 8), affects the IR spectrum only slightly, indicating, as one would expect, that this hydrogen bond is less strong than the hydrogen bond between an ACN molecule and the hydrogen atom of the OH group of the enol tautomer. As a consequence, the normal modes involving the amine group are not altered significantly upon inclusion of an explicitly hydrogen-bonded ACN solvent molecule in the calculations.

3.5. Comparison between Experimental and Theoretical Results. In Figure 9 we compare the experimental and theoretical spectra of HBT in ACN-d_3. For HBT in the electronic ground state, a perfect match between experiment and theory results (using COSMO) assuming HBT exists predominantly in the enol(Θ = 0°) conformer, i.e., with the intramolecular hydrogen bond connecting the hydroxyphenyl OH-group with the nitrogen of the benzothiazole moiety. As a result, the starting conditions of the photophysics of HBT are similar in TCE and in ACN. The outcome in TCE is dominated by a single route: ultrafast ESIHT from the enol*(Θ = 0°) S_1 state to the keto*(Θ = 0°) S_1 state, followed by the emission of a fluorescent photon, with which the keto(Θ = 0°) S_0 state is reached, and finally the enol(Θ = 0°) S_0 state results by intramolecular hydrogen back transfer. Upon reaching the enol*(Θ = 0°) S_1 state in ACN, however, HBT follows a multitude of reaction pathways. The electronic transition dipole moments μ_{el} of enol(Θ = 0°), enol(Θ = 180°), and keto(Θ = 180°) in the gas phase was calculated using DFT with the B3LYP density functional and the TZVP basis set and turn out to be of similar magnitude: μ_{el}[enol(Θ = 0°)] = 4.943692 D, μ_{el}[enol(Θ = 180°)] = 4.180663 D, and μ_{el}[keto(Θ = 180°)] = 5.249449 D. The steady-state emission spectra thus suggest a branching into enol* and keto* conformers of about equal probability. The fact that ESIHT of the enol*(Θ = 0°) to the keto*(Θ = 0°) state occurs with similar reaction rates in ACN-d_3 and in TCE, as evidenced by the appearance of keto*(Θ = 0°) vibrational marker modes within time resolution of 150 fs, means that twisting and ESIHT compete as equal reaction pathways on a femtosecond time scale.

Twisting in the electronic excited state followed by internal conversion is a well-known mechanism for molecules with ethylenic bonds, such as *trans*- and *cis*-stilbene[51−56] and retinal and coumaric acid chromophores in photoreceptor proteins.[57−59] The fate of the enol* conformer after twisting is indeed that of internal conversion back to the S_0 state, followed by reformation of the intramolecular hydrogen bond (there is only a small twisting energy barrier for the enol conformers, ultimately reaching the energetically most favorable enol(Θ = 0°) conformation). The fact that the lifetime of the S_1 keto*(Θ = 0°) state is also substantially shortened means that twisting and internal conversion to the electronic ground state are equally probable routes for the electronically excited keto conformers. Here HBT may either end up in the keto(Θ = 0°) conformer, which is energetically unstable and will rapidly convert back to enol(Θ = 0°), or will become keto(Θ = 180°), which is metastable because it is located on a local potential energy minimum. Only when a full 180° rotation around the twisting angle Θ occurs can the keto conformer convert back to the enol(Θ = 0°) by intramolecular hydrogen back transfer.

For HBT in ACN-d_3, the transient IR signatures in the fingerprint region at early pulse delay times are dominated by the keto*(Θ = 0°) marker bands. Even though the fluorescence spectra suggest that a substantial amount of enol* conformers exist in the S_1 state, no distinct marker modes have been detected, which may mean that the vibrational marker bands of the enol* conformers have smaller cross sections than those of the keto* conformers. We can compare with the vibrational fingerprint spectra calculated for HBT in the S_0 state. Figure 9 shows that for the keto(Θ = 180°) conformer, the vibrational transitions have cross sections that are significantly higher than the ones of the enol(Θ = 0°) and enol(Θ = 180°) conformers. Such behavior may occur in the electronic excited state as well. For now we refrain from further analyzing the excited state vibrational fingerprint modes of HBT.

The calculated spectra shown in Figure 9 also indicate that the single transient band at 1616 cm^{-1}, measured at long pulse delay of 120 ps, can be caused by the keto(Θ = 180°) conformer. It is less likely that the enol(Θ = 180°) conformer contributes, as one would expect, a doublet structure in this spectral region (see also Figure 8). Signatures of other fingerprint modes of the keto conformer will also contribute to the IR spectra between 1400 and 1550 cm^{-1}, but these will overlap with bleach signals of the enol(Θ = 0°) ground state. From the transient IR spectrum at 120 ps pulse delay, we conclude that upon excited state decay by internal conversion, likely caused by the intramolecular twisting,

the fate of the majority of HBT molecules is the return to the enol($\Theta = 0°$) electronic ground state. If enol conformers with other twisting angle values appear upon internal conversion, a rapid (within the time scale of vibrational cooling in ACN-d_3) conversion into the enol($\Theta = 0°$) conformer occurs. This is also true for those keto conformers with twisting angles $\Theta < 90°$, because keto($\Theta = 0°$) is unstable, and converts into enol($\Theta = 0°$) by intramolecular hydrogen back transfer. Keto conformers with twisting angles $\Theta > 90°$ on the other hand will relax to the keto($\Theta = 180°$) local minimum. We thus conclude that solvent-induced twisting in direct competition with ESIHT enables the transient generation of an HBT conformer, keto($\Theta = 180°$), with significant longer lifetimes than the other conformers.

We emphasize here that the mechanism for electronic excited state relaxation is controlled by the polar solvent. This can be contrasted with the observation of a shortened S_1-state lifetime of HBT keto*($\Theta = 0°$) in the gas phase (2.6 ps) compared to that in nonpolar cyclohexane (~100 ps).[45] In the gas phase, no excited-state enol* conformers have been observed, whereas we observe a fluorescence band in the UV region, likely from enol* conformers with twisting angles $\Theta \neq 0°$. In the gas phase, internal conversion has been ascribed to intramolecular twisting mechanisms causing a cleavage of the intramolecular hydrogen bond. In solution phase, the hydrogen bond cleavage is likely induced by the polar solvent medium. The polar solvent is also responsible for the increased stability of the keto($\Theta = 180°$) conformer, prolonging its lifetime. Most importantly, by use of femtosecond IR spectroscopy, we are able to identify a tautomer of HBT generated on picosecond time scales and assign it to the keto($\Theta = 180°$) conformer. This finding, together with the enol* fluorescence signature, makes a strong argument that, besides ESIHT, twisting plays a key role in the photophysics of HBT in ACN. These findings should propel excited state quantum mechanical/molecular mechanics calculations (incorporating the effects of the polar solvent) of HBT, with which one may tackle questions about the microscopic description of the reaction pathways and associated dynamics of enol* and keto* isomers, quantum yields for branching, and even precise determination of time scales for internal conversion of enol* and of keto* isomers with associated dependencies of twisting angles and solvent shell configurations.

4. CONCLUSION

We have investigated the ultrafast dynamics of HBT in the polar solvent ACN and in nonpolar TCE. The steady-state IR absorption indicates that in the electronic ground state, HBT predominantly exists in both solvents as the enol tautomer with an intramolecular hydrogen bond connecting the OH group of the hydroxyphenyl part with the nitrogen of the benzothiazole group. By contrast, the fluorescence spectra show that a clear difference exists in the photophysics of HBT in both solvents: whereas HBT in TCE performs ESIHT to the keto* tautomer followed by emission, in ACN both enol* and keto* emission occurs. In addition to that, the lifetimes of the electronic excited states of enol* and keto* tautomers are significantly shorter, evidencing an efficient internal conversion process. In combination with the femtosecond IR spectra, we conclude that in ACN HBT can follow two competing reaction pathways: intramolecular twisting around the central C−C bond connecting the hydroxyphenyl and benzothiazole moieties, as well as ESIHT converting enol* to keto*. Intramolecular twisting occurs for both enol* and keto* tautomers, inducing a recovery to the electronic ground state. Most conformers convert back to the enol conformer with the intramolecular hydrogen bond restored. In ACN, however, a keto conformer with its hydroxyphenyl and benzothiazole units twisted 180° around the central C−C persists for delay times up to at least 120 ps. As such we show that solvent control of branching of two different types of reactions, intramolecular hydrogen transfer versus intramolecular twisting, is at the heart of the different behavior of HBT in polar ACN compared to that in nonpolar TCE. This important finding of solvent control of reaction dynamics, we believe, should be explored and utilized in the design and optimization of photoinduced conformational changes in molecular switches.

AUTHOR INFORMATION

Corresponding Author
*E-mail address: nibberin@mbi-berlin.de.

ACKNOWLEDGMENT

This work benefitted from funding by a long term mission fellowship of the Egyptian government (O.F.M.), from supercomputer time from NERSC (V.S.B.), from funding by the National Science Foundation Grant CHE 0911520 (V.S.B.), and from valuable discussions with T. Elsaesser.

REFERENCES

(1) Bowman, J. M.; Schatz, G. C. *Annu. Rev. Phys. Chem.* **1995**, *46*, 169.
(2) Butler, L. J. *Annu. Rev. Phys. Chem.* **1998**, *49*, 125.
(3) Davis, H. F.; Lee, Y. T. *J. Phys. Chem.* **1992**, *96*, 5681.
(4) Banin, U.; Ruhman, S. *J. Chem. Phys.* **1993**, *98*, 4391.
(5) Pugliano, N.; Palit, D. K.; Szarka, A. Z.; Hochstrasser, R. M. *J. Chem. Phys.* **1993**, *99*, 7273.
(6) Baskin, J. S.; Zewail, A. H. *J. Phys. Chem.* **1994**, *98*, 3337.
(7) Pullen, S.; Walker, L. A.; Sension, R. J. *J. Chem. Phys.* **1995**, *103*, 7877.
(8) Davis, H. F.; Lee, Y. T. *J. Chem. Phys.* **1996**, *105*, 8142.
(9) Elles, C. G.; Crim, F. F. *Annu. Rev. Phys. Chem.* **2006**, *57*, 273.
(10) Crim, F. F. *Proc. Natl. Acad. Sci. U.S.A.* **2008**, *105*, 12654.
(11) Dugave, C.; Demange, L. *Chem. Rev.* **2003**, *103*, 2475.
(12) Nibbering, E. T. J.; Fidder, H.; Pines, E. *Annu. Rev. Phys. Chem.* **2005**, *56*, 337.
(13) Brixner, T.; Damrauer, N. H.; Niklaus, P.; Gerber, G. *Nature* **2001**, *414*, 57.
(14) Brixner, T.; Gerber, G. *ChemPhysChem* **2003**, *4*, 418.
(15) Herek, J. L.; Wohlleben, W.; Cogdell, R. J.; Zeidler, D.; Motzkus, M. *Nature* **2002**, *417*, 533.
(16) Siewertsen, R.; Renth, F.; Temps, F.; Sonnichsen, F. *Phys. Chem. Chem. Phys.* **2009**, *11*, 5952.
(17) Barbara, P. F.; Brus, L. E.; Rentzepis, P. M. *J. Am. Chem. Soc.* **1980**, *102*, 5631.
(18) Elsaesser, T.; Kaiser, W. *Chem. Phys. Lett.* **1986**, *128*, 231.
(19) Elsaesser, T.; Schmetzer, B.; Lipp, M.; Bauerle, R. J. *Chem. Phys. Lett.* **1988**, *148*, 112.
(20) Laermer, F.; Elsaesser, T.; Kaiser, W. *Chem. Phys. Lett.* **1988**, *148*, 119.
(21) Frey, W.; Laermer, F.; Elsaesser, T. *J. Phys. Chem.* **1991**, *95*, 10391.
(22) Lochbrunner, S.; Wurzer, A. J.; Riedle, E. *J. Chem. Phys.* **2000**, *112*, 10699.
(23) de Vivie-Riedle, R.; De Waele, V.; Kurtz, L.; Riedle, E. *J. Phys. Chem. A* **2003**, *107*, 10591.
(24) Lochbrunner, S.; Wurzer, A. J.; Riedle, E. *J. Phys. Chem. A* **2003**, *107*, 10580.

(25) Rini, M.; Dreyer, J.; Nibbering, E. T. J.; Elsaesser, T. *Chem. Phys. Lett.* **2003**, *374*, 13.
(26) Rini, M.; Kummrow, A.; Dreyer, J.; Nibbering, E. T. J.; Elsaesser, T. *Faraday Discuss.* **2003**, *122*, 27.
(27) Elsaesser, T. Ultrafast excited state hydrogen transfer in the condensed phase. In *Ultrafast Hydrogen Bonding Dynamics and Proton Transfer Processes in the Condensed Phase*; Elsaesser, T., Bakker, H. J., Eds.; Kluwer Academic Publishers: Dordrecht, The Netherlands, 2002.
(28) Ahlrichs, R.; Bär, M.; Häser, M.; Horn, H.; Kölmel, C. *Chem. Phys. Lett.* **1989**, *162*, 165.
(29) Becke, A. D. *Phys. Rev. A* **1988**, *38*, 3098.
(30) Perdew, J. P. *Phys. Rev. B* **1986**, *33*, 8822.
(31) Dunning, T. H., Jr. *J. Chem. Phys.* **1989**, *90*, 1007.
(32) Schäfer, A.; Huber, C.; Ahlrichs, R. *J. Chem. Phys.* **1994**, *100*, 5829.
(33) Neugebauer, J.; Herrmann, C.; Luber, S.; Reiher, M. SNF 4.0 - A program for the quantum chemical calculation of vibrational spectra; URL: http://www.reiher.ethz.ch/software/snf.
(34) Neugebauer, J.; Reiher, M.; Kind, C.; Hess, B. A. *J. Comput. Chem.* **2002**, *23*, 895.
(35) Bickley, W. G. *Math. Gazette* **1941**, *25*, 19.
(36) Brehm, G.; Reiher, M.; Schneider, S. *J. Phys. Chem. A* **2002**, *106*, 12024.
(37) Neugebauer, J.; Hess, B. A. *J. Chem. Phys.* **2003**, *118*, 7215.
(38) Reiher, M.; Brehm, G.; Schneider, S. *J. Phys. Chem. A* **2004**, *108*, 734.
(39) ftp://ftp.chemie.uni-karlsruhe.de/pub/jbasen.
(40) Klamt, A.; Schüürmann, G. *J. Chem. Soc., Perkin Trans. 2* **1993**, 799.
(41) Li, G.-Y.; Zhao, G.-J.; Liu, Y.-H.; Han, K.-L.; He, G.-Z. *J. Comput. Chem.* **2010**, *31*, 1759.
(42) Humphrey, W.; Dalke, A.; Schulten, K. *J. Mol. Graph.* **1996**, *14*, 33.
(43) Li, R. D.; Keith, T.; Millam, J.; Eppinett, K.; Hovell, L. W.; Gilliland, R. *Gaussview* version 5.0.8; Gaussian, Inc.: Wallingford, CT, 2008.
(44) Hamm, P.; Ohline, S. M.; Zinth, W. *J. Chem. Phys.* **1997**, *106*, 519.
(45) Barbatti, M.; Aquino, A. J. A.; Lischka, H.; Schriever, C.; Lochbrunner, S.; Riedle, E. *Phys. Chem. Chem. Phys.* **2009**, *11*, 1406.
(46) Aquino, A. J. A.; Lischka, H.; Hättig, C. *J. Phys. Chem. A* **2005**, *109*, 3201.
(47) Becke, A. D. *J. Chem. Phys.* **1993**, *98*, 5648.
(48) Lee, C. T.; Yang, W. T.; Parr, R. G. *Phys. Rev. B* **1988**, *37*, 785.
(49) Köhn, A.; Hättig, C. *J. Chem. Phys.* **2003**, *119*, 5021.
(50) Ríos, M. A.; Ríos, M. C. *J. Phys. Chem. A* **1998**, *102*, 1560.
(51) Lienau, C.; Heikal, A. A.; Zewail, A. H. *Chem. Phys.* **1993**, *175*, 171.
(52) Sension, R. J.; Repinec, S. T.; Szarka, A. Z.; Hochstrasser, R. M. *J. Chem. Phys.* **1993**, *98*, 6291.
(53) Schroeder, J.; Schwarzer, D.; Troe, J.; Vöhringer, P. *Chem. Phys. Lett.* **1994**, *218*, 43.
(54) Szarka, A. Z.; Pugliano, N.; Palit, D. K.; Hochstrasser, R. M. *Chem. Phys. Lett.* **1995**, *240*, 25.
(55) Schroeder, J.; Steinel, T.; Troe, J. *J. Phys. Chem. A* **2002**, *106*, 5510.
(56) Takeuchi, S.; Ruhman, S.; Tsuneda, T.; Chiba, M.; Taketsugu, T.; Tahara, T. *Science* **2008**, *322*, 1073.
(57) Schoenlein, R. W.; Peteanu, L. A.; Mathies, R. A.; Shank, C. V. *Science* **1991**, *254*, 412.
(58) Herbst, J.; Heyne, K.; Diller, R. *Science* **2002**, *297*, 822.
(59) Heyne, K.; Mohammed, O. F.; Usman, A.; Dreyer, J.; Nibbering, E. T. J.; Cusanovich, M. A. *J. Am. Chem. Soc.* **2005**, *127*, 18100.